Chapter 4

Electrochemical sensing of glucose and hydrogen peroxide using a self-assembled bis(acetylacetonato)oxovanadium(IV) complex modified gold electrode

4.1. Introduction

Green plants produce glucose by the reduction of carbon dioxide and the metabolic oxidation of glucose sustains all living beings.[1] Glucose is transported to cells via insulin in the bloodstream. The human body maintains blood glucose levels at a concentration of 4 - 8 mM (70 -120 mg dL^{-1}).[2] An abnormal blood sugar level causes diabetes which represents a leading cause of several complications for human health like complications to retina, circulatory system, kidneys etc.[3] To manage the blood glucose level patients need to monitor blood glucose level on a regular basis. On the other hand, hydrogen peroxide (H_2O_2) is a simple but very important molecule in nature, and is extensively used as an oxidizing agent in the food and chemical industries.[4] Moreover, H_2O_2 is one of the most important markers for oxidative stress and also acts as a precursor in the formation of highly reactive and potentially harmful hydroxyl radicals.[5, 6] Therefore, the accurate determination of glucose and H_2O_2 is of practical importance. Several analytical techniques have been carried out for the determination of glucose and H_2O_2 *viz*, titrimetry, spectrometry, fluorometry, chemiluminescence and electrochemical methods.[7-10] Amongst them, the electrochemical approach is promising because of its higher sensitivity and selectivity, lower detection limit, faster response time, better long term stability and cheap.[11] For the detection of glucose and H_2O_2 both enzymatic [12,13] and non-enzymatic [14,15] sensor have been developed. First, second and third generation enzymatic glucose sensors has been developed due to overcome the disadvantages. The third generation sensor still in their infancy, yet some of them based on nano-mesoporous electrode surface show some promise.[16] There are still some disadvantages of enzyme-based determination. Examples include complicated enzyme immobilization, critical operating conditions viz. optimum temperature and pH, chemical instability, poor reproducibility and high cost.[17] To solve these problems, fourth generation enzyme-free sensors have been developed for glucose oxidation and H_2O_2 reduction. In general, these electroactive analytes can be oxidized or reduced directly at ordinary solid electrodes. However, owing to their high over-potential, slow electrode kinetics and poor measurement stability caused by poisoning from the intermediate products restricts the performance of this electrodes.[18] Therefore; current efforts have mainly focused on discovering new materials with high catalytic activity and good stability in order to

construct non-enzymatic sensors. The fabrication of a wide variety of nanomaterials have been introduced for the selective and sensitive detection of glucose [19,20] as well as H_2O_2.[21,22] On the other hand very limited numbers of metal complexes have been used so far for the electrochemical sensing of glucose and H_2O_2. Complexes with reversible redox capabilities such as cobalt phthalocyanine,[23] nickel curcumin,[24] nickel porphyrine,[25] copper hexacyanoferrate [26] have been used for the effective electrocatalytic sensing for glucose whereas cobalt tetrasulfophthalocyanine,[27] cobalt tetraruthenated porphyrin,[28] cobaltoxyhydroxide,[22] DNA-Cu^{2+} complex [29] for H_2O_2 sensing. Instead of cobalt, nickel and copper containing complexes no other earth abundant transition metal complexes have been reported for the electrochemical sensing of glucose and H_2O_2. Among first d-block transition-metal series, vanadium has critical roles in various chemical and biological processes.[30] Presently the catalytic role of vanadium in higher oxidation states (IV and V) has received much attention after the discovery of vanadium dependent enzymes such as vanadium-iron nitrogenise of Azotobacter vinelandii and vanadium haloperoxidases in marine algae.[31] Several oxovanadium and dioxovanadium complexes acts as functional models of haloperoxidases and catalyze oxyhalogenation of various aromatic substrates.[32] Instead of these, oxovanadium complexes have also been used to catalyze several reactions such as the oxidation of olefins, alcohols,[33] aldehydes,[34] tertiary amine,[35] thiols,[36] hydrogen peroxide,[37] epoxidation [38] and oxidative coupling reaction.[39] Apart from their role as catalyst, there is a widespread interest on the biological chemistry of vanadium compounds because of its perceived potential for the development as a pharmacologic agent for the treatment of diabetes mellitus.[40] Extensive literature review shows that among large number of oxovanadium compounds, only *bis*(acetylacetonato)oxovanadium, $[VO(acac)_2]$, exhibits the greatest capacity to enhance insulin receptor kinase activity in cells associated with a significant decrease in plasma glucose concentration.[41] Posner and co-workers showed that vanadate reacted with H_2O_2 stimulated the phosphorylation of the insulin receptor in endosomes with efficiency comparable to that of insulin.[42] Makinan and Brady showed that $[VO(acac)_2]$ stimulate the uptake of glucose by serum-starved 3T3-L1 adipocytes in the presence of bovine serum albumin.[43]

These rich catalytic and pharmacological properties of oxovanadium complexes encourage us to prepare the $[VO(acac)_2]$ complex modified gold electrode and study the non-enzymatic electrochemical sensing behaviour for glucose and hydrogen peroxide. To the best of our knowledge, this is the first report of sensing both glucose and hydrogen peroxide by the same metal complex modified electrode at neutral pH. The oxovanadium(IV) complex modified gold electrode shows excellent electrocatlytic activity and exhibit notable sensing performance towards glucose and H_2O_2. The kinetics of glucose oxidation and hydrogen peroxide reduction was also examined in detail. More importantly, we demonstrate successfully its application for the quantitative detection of glucose in human blood sample and H_2O_2 in processed milk. 0.1M phosphate buffer solution (PBS) was prepared by mixing 0.1 M $NaClO_4$ and 0.01 M H_3PO_4 and the pH values were adjusted by the addition of 0.11 M NaOH using Smalley's method.[44]

4.2. Experimental

4.2.1. Construction of $[VO(acac)_2]$-PATP modified gold electrode

A gold electrode was polished with wet α-alumina (0.5 μm) on a flat polishing pad for 10 minutes and rinsed several times with doubly distilled water. The cleanliness of the gold electrode surface was ascertained by recording the repetitive cyclic voltammograms in 0.5 M H_2SO_4 between - 0.2 and + 1.5 V *versus* Ag/AgCl with 0.1 V/s scan rate until a steady characteristic gold oxide cyclic voltammogram was obtained.[45] The electrode was then rinsed with doubly distilled water and immersed in 1.0 mM ethanolic solution of 4-aminothiophenol (4-ATP) for 24 hours. The 4-ATP was self-assembled over the gold electrode surface via gold-sulfur interaction and the modified electrode 4-ATP-Au was thoroughly washed with double distilled water. Thereafter, the modified gold electrode was dipped into 1.0 mM isonicotinic acid solution for 4 hours under stirring condition and 4-(pyridine-4′-amido)thiophenol modified gold electrode (PATP-Au) was formed. After washed with double distilled water PATP-Au electrode was immersed into an ethanolic solution of 1.0 mM $[VO(acac)_2]$ and stirred for 2 hours so that the pyridine nitrogen of PATP-Au was able to form adduct with the vacant coordination site of vanadium in $[VO(acac)_2]$. The finally modified electrode $[VO(acac)_2]$-4-PATP-Au was washed thoroughly with distilled water and dried in air for further use.

4.3. Results and discussion

4.3.1. Characterization of modified gold electrode

The step wise modification and surface morphology of the gold electrode were characterized by FE-SEM and elemental mapping (Fig. 4.1). From the SEM images, it can be seen that the surface of the bare (Fig. 1A) gold electrode was smooth and remains almost the same (Fig. 1B) after modification with 4-aminothiophenol (4-ATP), suggesting well-ordered and densely packed layer formation. However, the surface morphology of the 4-ATP-Au electrode was changed to a uniform wire-like structure (Fig. 1C) after a Schiff base condensation reaction between isonicotinic acid and 4-ATP-Au. After the subsequent immobilization of $[VO(acac)_2]$ on the 4-PATP-Au electrode (Fig. 1D), $[VO(acac)_2]$-4-PATP modified gold electrode shows very rough and porous surface which is favourable for the electrocatalytic activity.

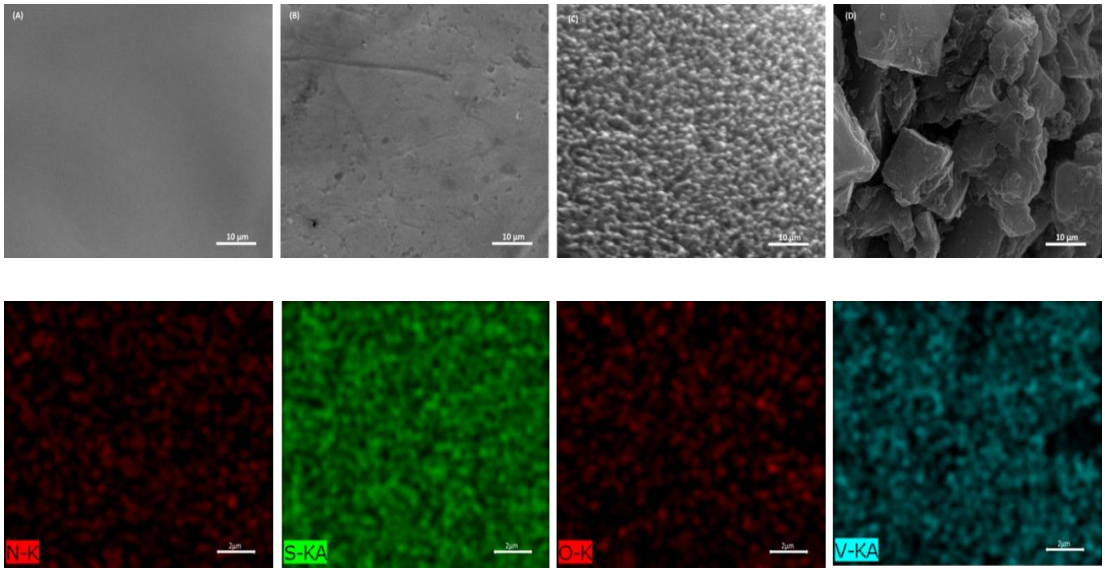

Fig. 4.1. FE-SEM images (top) of different electrode systems bare Au (A), ATP -Au (B), PATP- Au (C), $[VO(acac)_2]$-4-PATP modified gold electrode (D) (10 µm scale bar) and elemental mapping images (bottom) of $[VO(acac)_2]$-4-PATP modified gold electrode(1µm scale bar).

Elemental mapping images confirms the immobilization of $[VO(acac)_2]$ over self-assembled monolayer 4-PATP modified gold electrode.[46] The modification process was

also monitored by cyclic voltammetry and electrochemical impedance spectroscopy using $[Fe(CN)_6]^{3-/4-}$ as redox probe in 0.1 M PBS solution at pH 7.0 (Fig. 4.2). The cyclic voltammogram of 0.5 mM $[Fe(CN)_6]^{4-}$ exhibits an electrochemically reversible redox couple on bare electrode (Fig. 4.2A).

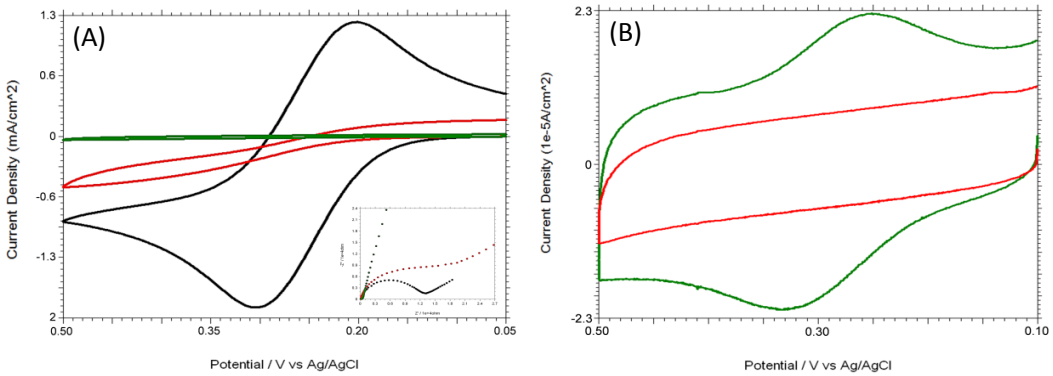

Fig. 4.2. (A) Cyclic voltammograms and Nyquist plot ($-Z^{//}$ versus $Z^{/}$) (inset) of 0.5 mM $K_4[Fe(CN)_6]$ in 0.1M PBS at pH 7 using different working electrode [bare Au (black), ATP -Au (red), PATP- Au (green)]. (B) Cyclic voltammograms in 0.1M PBS at pH 7 before (red) and after (green) immobilization of $[VO(acac)_2]$.

After modification the gold electrode with 4-aminothiophenol, the cyclic voltammogram of $[Fe(CN)_6]^{4-}$ exhibit an irreversible couple with low current height than bare gold electrode. The current height decreased even more when 4-(pyridine-4′-amido)thiophenol (PATP) modified Au was used as working electrode. These CV results indicated that the electronic communication between gold and $[Fe(CN)_6]^{4-}$ is blocked due to PATP film formation.[46] In the Nyquist plot (Fig. 4.2A inset), the diameter of the semi-circle increases gradually when stepwise modification on the gold electrode surface was carried out. The observed trend is due to the fact that the modified electrode blocked the electron transfer for the redox reaction of $[Fe(CN)_6]^{4-}$. Electrochemical impedance measurement supports the CV results. The fabrication of $[VO(acac)_2]$ over PATP- Au electrode was confirmed by taking a comparative cyclic voltammogram for PATP-Au and $[VO(acac)_2]$-4-PATP-Au in 0.1 M PBS buffer at pH 7.0 (Fig. 4.2B). A quasireversible $[V^{V}O(acac)_2]^{+}$ /$[V^{IV}O(acac)_2]$ redox couple at + 0.33 V supports the fabrication of $[VO(acac)_2]$-4-PATP-Au electrode.[46]

4.3.2. Electrocatalytic oxidation of glucose and reduction of H_2O_2

Figure 4.3A and 4.3B shows the cyclic voltammograms (CV) of 0.1 mM glucose and 0.5 mM hydrogen peroxide, respectively in 0.1 M PBS at pH 7.0 using bare Au, PATP-Au and $[VO(acac)_2]$-4-PATP-Au electrodes. An irreversible oxidation of glucose occurred at + 0.65 V by the $[VO(acac)_2]$-PATP-Au electrode with large increase of current whereas no such prominent peak was observed with bare and PATP-Au electrode (Fig. 4.3A). In absence of glucose no such oxidation peak was observed at $[VO(acac)_2]$-4-PATP-Au electrode (Fig. 4.4A).

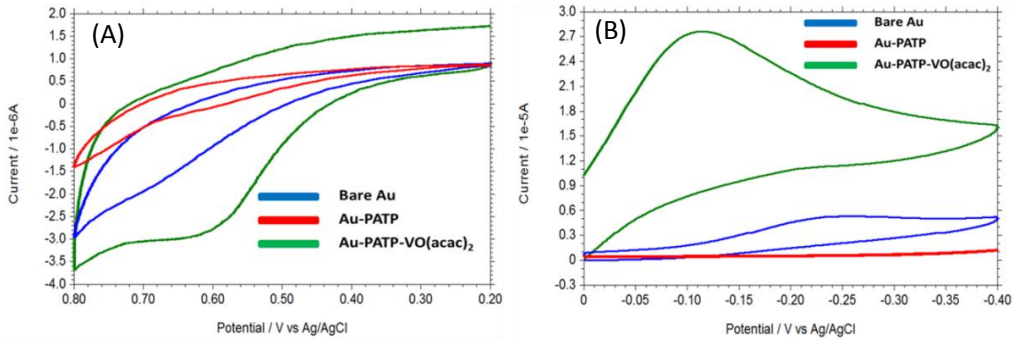

Fig. 4.3. Cyclic voltammograms obtained with bare, PATP and $[VO(acac)_2]$-4-PATP modified gold electrode in 0.1 mM glucose (A) and 0.5 mM hydrogen peroxide (B) in 0.1 M PBS solution (pH 7.0).

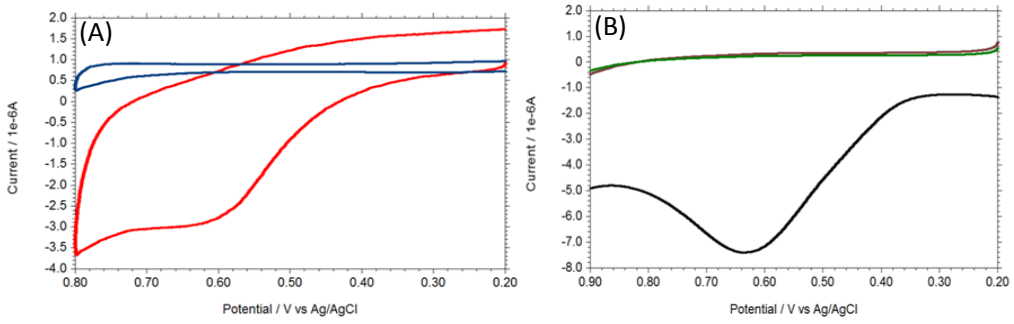

Fig. 4.4. (A) Overlaid CV obtained with (red curve) and without (blue curve) 0.1 mM glucose at the $[VO(acac)_2]$-4-PATP-Au electrode in 0.1 M PBS solution (pH = 7.0). (B) Overlaid DPV obtained with bare (brown curve), PATP (green curve) and $[VO(acac)_2]$-4-PATP (black curve) modified gold electrode in 0.1 mM glucose in 0.1 M PBS solution (pH = 7.0).

This behaviour indicate the electrocatalytic activity of $[VO(acac)_2]$-4-PATP modified gold electrode towards glucose oxidation. DPV experiment (Fig. 4.4B) gives a prominent glucose oxidation peak only at $[VO(acac)_2]$-4-PATP-Au electrode under similar condition and supports the results obtained by CV (Fig. 4.3A). The catalytic pathway of glucose oxidation can be describe on assuming that the electrochemical process is initiated by the non-covalent interaction of glucose with surface bound $[VO(acac)_2]$. During anodic scan $[V^{IV}O(acac)_2]^0$ is oxidized to the catalytically active $[V^{V}O(acac)_2]^+$ complex over PATP modified gold electrode. $[V^{IV}O(acac)_2]^0 \rightarrow [V^{V}O(acac)_2]^+ + e^-$ .....(Eq. a). Once $[V^{V}O(acac)_2]^+$ is formed, glucose is oxidized on the modified electrode surface *via* the following reactions.

$[V^{V}O(acac)_2]^+ + \text{glucose} \rightarrow \text{Intermediate} + [V^{IV}O(acac)_2]^0$ ...(Eq. b)

$[V^{V}O(acac)_2]^+ + \text{intermediate} \rightarrow \text{gluoconolactone} + [V^{IV}O(acac)_2]^0$....(Eq. c).

The cyclic voltammogram of H_2O_2 (Fig. 4.3B) in 0.1 M PBS (pH 7.0) shows a cathodic response at around - 0.24 V at bare gold electrode. When the gold electrode was modified by 4-(pyridine-4′-amido)thiophenol, no current response was observed. After modification with $[VO(acac)_2]$, a sharp peak was observed around – 0.11 V with sufficiently high current response during the cathodic scan. In absence of H_2O_2 no such reduction peak was obtained at $[VO(acac)_2]$-4-PATP-Au electrode under similar condition (Fig. 4.5).

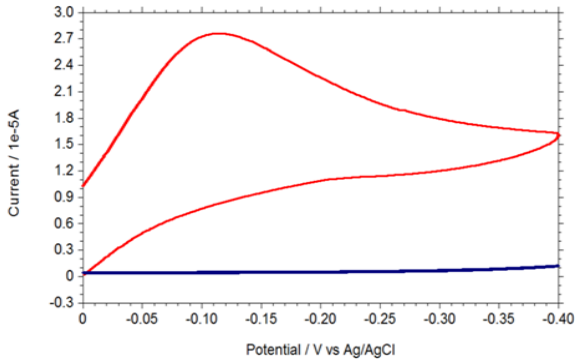

Fig. 4.5. Overlaid cyclic voltammogram obtained with (red curve) and without (blue curve) 0.5 mM H_2O_2 at the $[VO(acac)_2]$-4-PATP-Au electrode in 0.1 M PBS solution (pH = 7.0).

Through these observations it was clear that oxovanadium (IV) complex exhibit enhanced electrocatalytic efficiency by their adhesion on the PATP-Au electrode. This is rationalized by a high ability of the $[VO(acac)_2]$ to transfer electrons involved in the catalytic reaction and sense the presence of H_2O_2 electrochemically. A common two electron redox mechanism is proposed for hydrogen peroxide reduction at the $[VO(acac)_2]$-4-PATP-Au electrode surface in which a substantial interaction with H_2O_2 and vanadium promotes the electron transfer and is shown by the following reactions.

$$[V^{IV}O(acac)_2]^0 + H_2O_2 \rightarrow H_2O + [V^{V}O(acac)_2]^+ \quad \text{... (Eq. d)}$$

$$[V^{V}O(acac)_2]^+ + e^- \rightarrow [V^{IV}O(acac)_2]^+ \quad \text{.....(Eq. e)}$$

Electrochemical impedance spectroscopy was also carried out for glucose and H_2O_2 using bare and modified gold electrodes (Fig. 4.6). The diameter of the semicircle observed in the Nyquist plot corresponds to charge transfer resistance, R_{ct}; the smaller the semi-circle, faster is the charge transfer. Fig. 4.6A and 4.6B shows that the diameter of the semicircle (R_{ct}) changes upon modification of gold electrode surface.

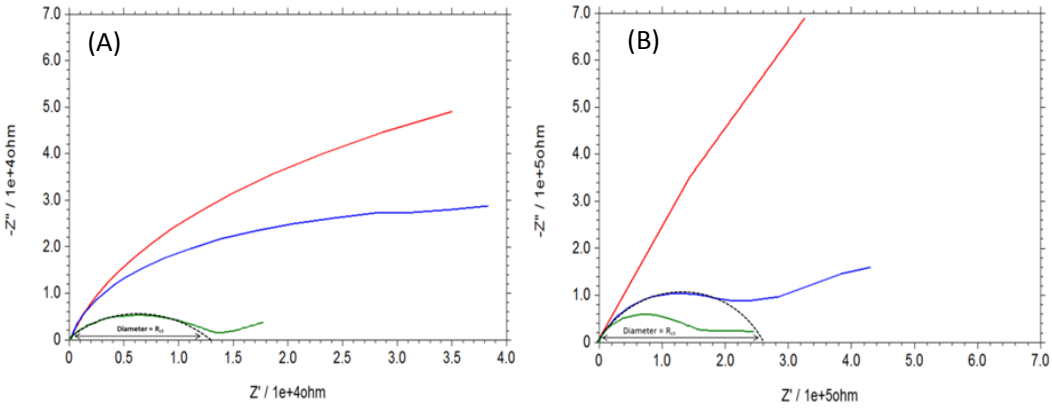

Fig. 4.6. Overlaid Nyquist plot of 0.1 mM glucose (A) and 0.5 mM H_2O_2 (B) in 0.1 M phosphate buffer solution (pH = 7.0) using bare and modified gold electrodes. E_{ac} = 10 mV, frequency range: 0.01-100000 Hz. For glucose, bare Au (blue curve), $R_{ct} = 4.0 \times 10^4$ Ω; PATP - Au (red curve), $R_{ct} = 4.8 \times 10^4$ Ω; $[VO(acac)_2]$-4-PATP-Au (green curve, $R_{ct} = 1.3 \times 10^4$ Ω and for H_2O_2, bare Au (blue curve), $R_{ct} = 2.6 \times 10^5$ Ω; PATP-Au (red curve), $R_{ct} = 6.4 \times 10^5$ Ω; $[VO(acac)_2]$-4-PATP-Au (green curve), $R_{ct} = 1.2 \times 10^5$ Ω.

The R_{ct} values for 0.1 mM glucose oxidation and 0.5 mM H_2O_2 reduction at $[VO(acac)_2]$-4-PATP-Au electrode in 0.1 M PBS at pH 7.0 were 1.3 $\times 10^4$ Ω and 1.2 $\times$ 10^5 Ω respectively, which were quite smaller than the R_{ct} obtained at PATP modified and bare gold electrode. The observed results are due to the fact that the $[VO(acac)_2]$ modified electrode ease the electron transfer rate for the oxidation of glucose and reduction of H_2O_2 whereas the 4-PATP modified gold electrode blocked the electron transfer. Electrochemical impedance measurements clearly indicate that $[VO(acac)_2]$-4-PATP modified gold electrode has lower resistance as compared to bare or 4-PATP modified gold electrodes. This study supports the CV results and reveals that the $[VO(acac)_2]$-4-PATP-Au electrode is an efficient electrocatalyst for the oxidation of glucose and reduction of hydrogen peroxide.

4.3.3. Determination of glucose and H_2O_2

Based on optimized conditions, determination of glucose and H_2O_2 were performed using chronoamperometry. Fig. 4.7 shows the chronoamperometry curves of glucose with different concentration.

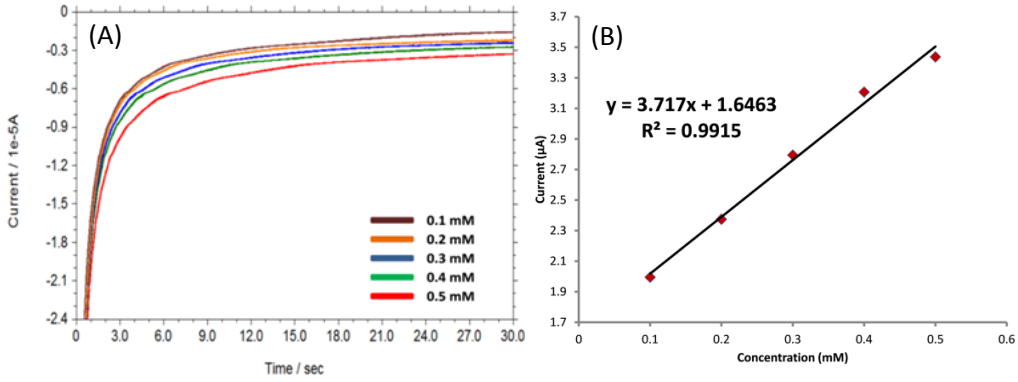

Fig. 4.7. (A) Chronoamperograms with increasing concentration of glucose (0.1 to 0.5 mM) in 0.1 M PBS (pH 7.0) at $[VO(acac)_2]$-4-PATP-Au electrode at + 0.65 V *vs* Ag/AgCl. LOD= 0.1 µM. (B) Plot of resulting current in chronoamperometry at 30 seconds *versus* concentration of glucose (0.1 – 0.5 mM).

The oxidation peak current of glucose was linear with its concentration in the range of 0.1 – 0.5 mM (Fig. 4.7B). The regression equation was I = 3.717 C + 1.646 (R^2 = 0.99), with a detection limit of 0.1 µM (S/N = 3).

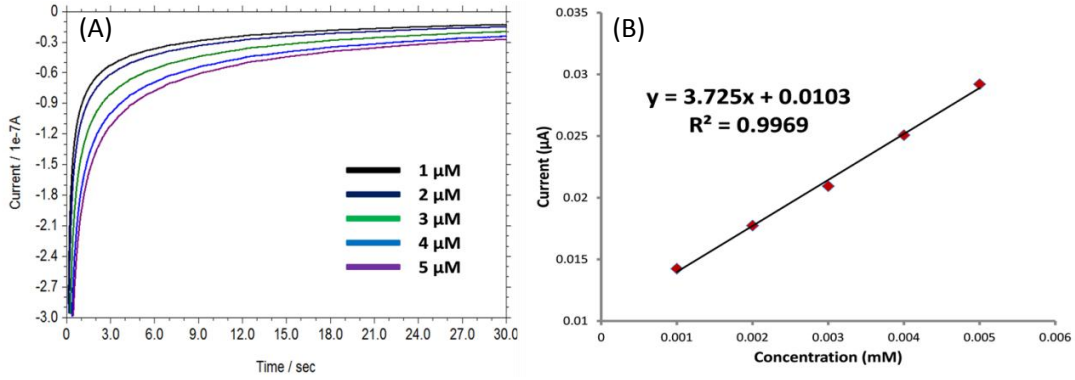

Fig. 4.8. (A) Chronoamperograms with increasing concentration of glucose (1.0 µM to 5.0 µM) in 0.1 M PBS (pH 7.0) at [$VO(acac)_2$]-4-PATP-Au electrode at + 0.65 V *versus* Ag/AgCl. (B) Plot of concentration of glucose *versus* oxidation peak current. Detection limit 0.1 µM (S/N = 3).

Exactly same detection limit was obtained in the lower concentration range of glucose (1.0 µM to 5.0 µM) (Fig. 4.8). The detection limit was further confirmed by differential pulse voltammetry (Fig. 4.9).

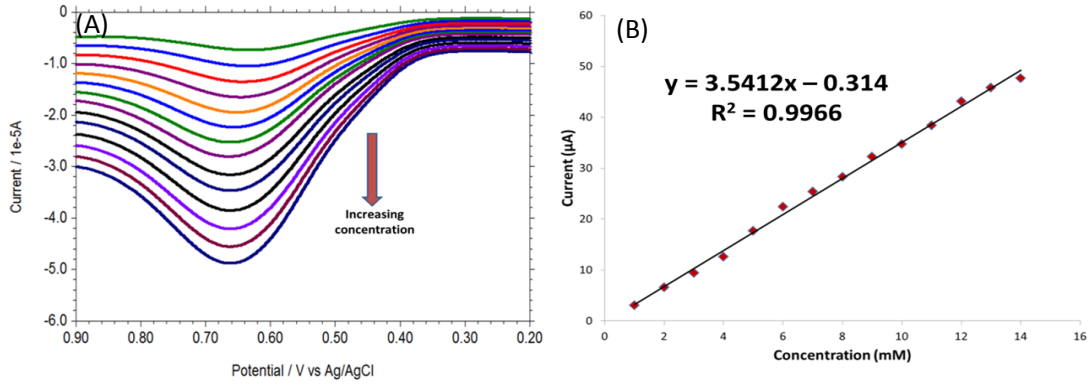

Fig. 4.9. (A) Overlaid Differential pulse voltammogram with increasing glucose concentration (1-14 mM) in 0.1 M PBS (pH = 7.0) at [$VO(acac)_2$]-4-PATP-Au electrode (B) Plot of current as a function of concentration of glucose with linear trend line (R^2 > 0.99).

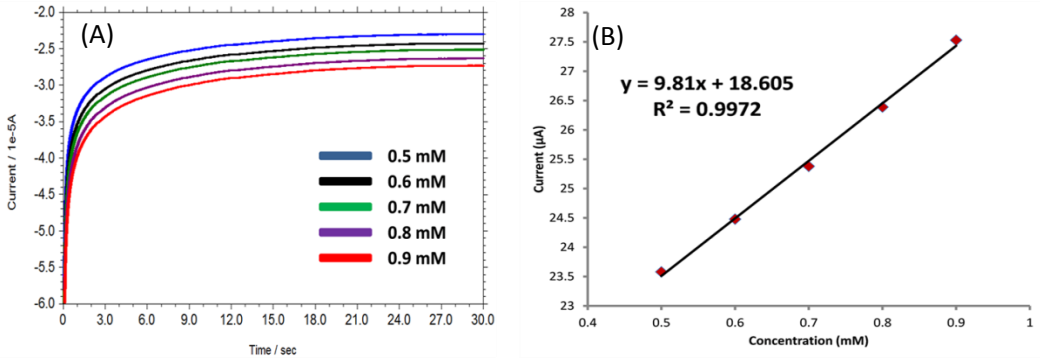

Fig. 4.10. (A) Chronoamperograms with increasing concentration of H_2O_2 (0.5 to 0.9 mM) in 0.1 M PBS (pH 7.0) at $[VO(acac)_2]$-4-PATP-Au electrode at - 0.11 V *versus* Ag/AgCl. LOD = 0.03 µM. (B) Plot of resulting current in chronoamperometry at 30 seconds *versus* concentration of H_2O_2 (0.5 – 0.9 mM).

Fig. 4.10 and 4.11 show the chronoamperogram response for H_2O_2 in the concentration range of 0.5 – 0.9 mM and 20 – 40 µM. The current was linearly proportional to its higher concentration range with a linear regression equation I = 9.81 C + 18.61 (R^2 = 0.99) (Fig. 4.10B) and in the low concentration range with a linear regression equation I = 9.81 C + 0.02 (R^2 = 0.99) (Fig. 4.11B). The detection limit for H_2O_2 was 0.03 µM (S/N = 3). The detection limit was further confirmed using CV results (Fig. 4.12A and 4.12B).

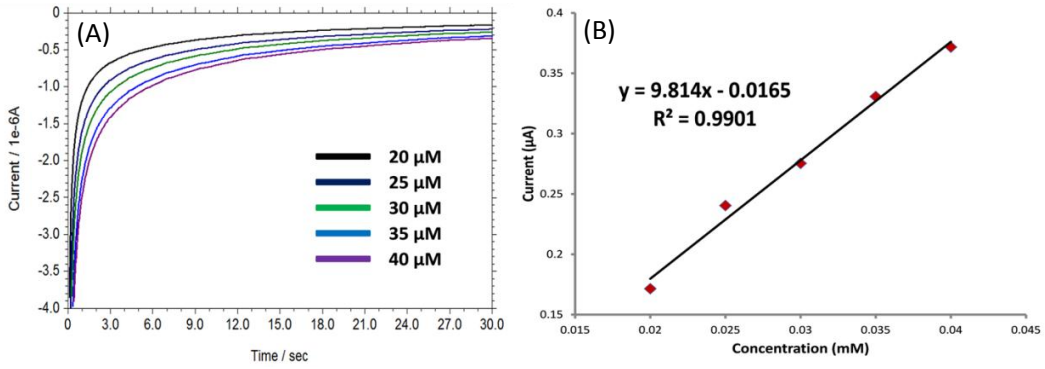

Fig. 4.11. (A) Chronoamperograms with increasing concentration of H_2O_2 (20 to 40 µM) in 0.1 M PBS (pH 7.0) at $[VO(acac)_2]$-4-PATP-Au electrode at - 0.11 V *versus* Ag/AgCl. (B) Plot of concentration of H_2O_2 *versus* reduction peak current. Detection limit 0.03 µM (S/N = 3).

Table 4.1. Comparative account of different non-enzymatic electrochemical sensors for glucose and hydrogen peroxide.

Sensor	Glucose				Hydrogen peroxide				
	Linear range (mM)	Detection limit (μM)	Applied voltage (V, *versus* Ag/AgCl)	Medium	Linear range (mM)	Detection limit (μM)	Applied voltage (V, *versus* Ag/AgCl)	Medium	Ref
Cu@M-Chit-CNT/GCE	0.0005-1 .0	0.05	+ 0.5	NaOH	0.0001 -1.0	0.025	- 0.25	PBS (pH 7.0)	1
Cu_2O/GNs/GCE	0.3 – 3.3	3.3	+ 0.60	KOH	0.3-7.8	20.8	-0.4	PBS (pH 7.4)	2
CQDs/O_h Cu_2O/Nafion/GCE	0.02-4.3	8.4	+ 0.60	NaOH	0.005-5.3	2.8	-0.2	PBS (pH 7.4)	3
Mn_3O_4/3DG	0.1 – 8	10	+0.4 0	NaOH					4
Au nanocoral/Au	0.05 – 30.0	10	+0.2	PBS (pH 7.4)					5
Au NW	1– 8	0.05	-0.16	PBS (pH 9.2)					6
CoPcTs/PNPGC	0.25 – 20	100	-	NaOH					7
Ni(II)-Curcumin/GC	0.001 - 10	0.1	+0.35	NaOH					8
poly[NiTRP]/GCE	0.0025-1.0	360	+ 0.47	NaOH					9
CuHCF-AuNP/graphite wax	0.0086-1.2	0.13	+ 0.59	KOH					10
Chitosan/AgNPs-G nano composite/GCE					0.1 - 10	7 .0	-0.3	PBS (pH 7.4)	11
Ag-MnOOH-GO/GCE					0.0005 -17.8	0.2	-0.2	PBS (pH 7.2)	12
CuO-SiNWs/GCE					0.01-13.18	1.6	-0.3	PBS (pH 7.0)	13
CoOOH nanosheet/Co foil/Au					0-1.6	40	+ 0.1	NaOH	14
Fe(III)-MPBA-nanoporous gold/Au					0.0009 – 0.5	0.001	-		15
DNA-Cu(II)/GCE					0.0008 – 4.5	0.25	-0.25		16
$[VO(acac)_2]$-PATP/Au	0.1-0.5	0.1	+0.65	PBS (pH 7.0)	0.5 – 0.9	0.03	- 0.11	PBS (pH 7.0)	This work

[Cu_2O/GNs: Cu_2O nanocubes wrapped by graphene nanosheets); CQDs/O_h Cu_2O: carbon quantum dots (CQDs)/octahedral cuprous oxide(Cu_2O) nanocomposites; 3DG: Three dimensional graphene; Au NW: gold nanowire array electrode; CoPcTs (cobalt (II) phthalocyanine tetrasulfonate); PNPGC: polypyrrole nanofiber onto pencil graphite electrode; poly[NiTRP]: polymeric tetraruthenated nickel porphyrin films; CuHCF: Cu hexacyano ferrate; MPBA: 4-mercapto-3-(phosphonomethylamino) butanoic acid, AgNPs-G: Ag nanoparticles-graphene; Ag-MnOOH-GO: Silver nanoparticle- manganese oxyhydroxide- graphene oxide; SiNWs: silicon nanowires.]

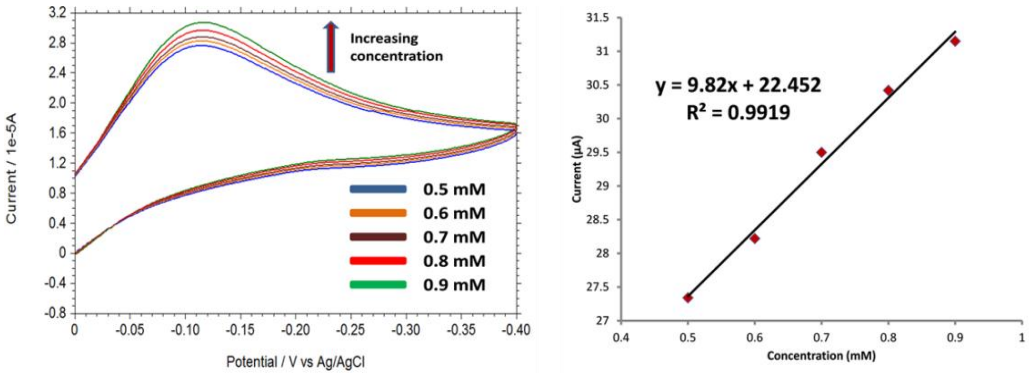

Fig. 4.12. (A) Overlaid cyclic voltammograms with increasing hydrogen peroxide concentration in 0.1 M PBS (pH = 7.0) at $[VO(acac)_2]$-4-PATP-Au electrode (B) Plot of current as a function of concentration of hydrogen peroxide with linear trend line ($R^2 > 0.99$).

Table 4.1 shows a comparison of the proposed electrochemical method and other modified electrodes reported for the electrocatalytic oxidation of glucose and reduction of H_2O_2. It can be seen that the detection limit obtained in the present system are comparable with some reported metal complex modified electrodes and quite better than the metal nanoparticle / nanocomposite modified electrodes.

4.3.4. Effect of scan rate and kinetic analysis for glucose oxidation and hydrogen peroxide reduction

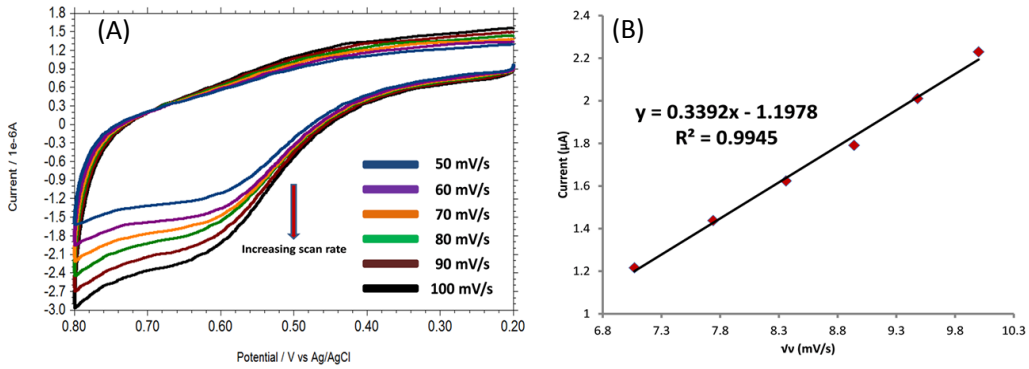

Fig. 4.13. (A) Cyclic voltammograms of 0.1 mM glucose in 0.1 M PBS (pH 7.0) at different scan rate using $[VO(acac)_2]$-4-PATP-Au electrode (B) Plot of oxidation peak current *versus* square root of scan rate.

The influence of the scan rate on the electrocatalytic oxidation of glucose (Fig. 4.13A) and the reduction of H_2O_2 (Fig. 4.14A) at $[VO(acac)_2]$-4-PATP-Au were investigated using cyclic voltammetry.

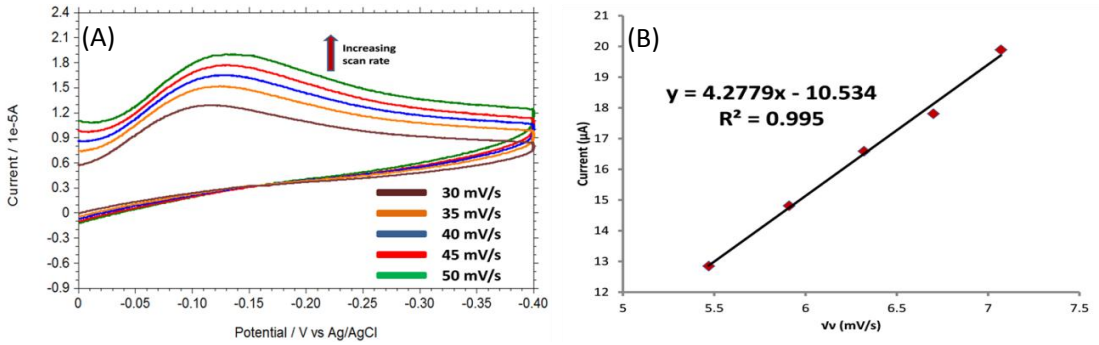

Fig. 4.14. (A) Cyclic voltammograms of 0.5 mM H_2O_2 in 0.1 M PBS (pH 7.0) at different scan rate using $[VO(acac)_2]$-4-PATP-Au electrode (B) Plot of oxidation peak current of 0.5 mM H_2O_2 *versus* square root of scan rate.

The results showed that on increasing the scan rates the oxidation peak potential of glucose and the reduction potential of hydrogen peroxide shifts to more positive and

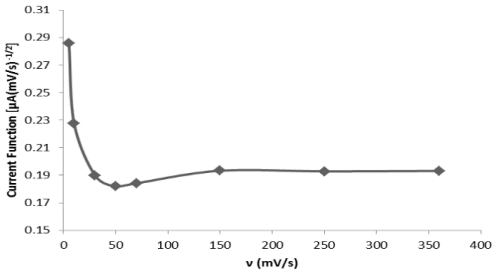

Fig. 4.15. Plot of scan rate –normalized current ($I_p/\nu^{1/2}$) with scan rate (ν).

more negative values, respectively, confirming the kinetic limitation of the electrochemical reaction.[27] Moreover, a plot of scan rate -normalized current ($I_{pa}/\nu^{1/2}$) *versus* scan rate (Fig. 4.15) shows a shape typical of EC catalytic process for glucose oxidation.[47] In addition, a plot of the peak current (I_{pa}) *versus* the square root of the scan rate ($\sqrt{\nu}$) (Fig. 4.13B) in the range of 50 -100 mV/s was found to be linear following the linear regression equation I_{pa} (μA) = 0.3392 ν (mVs^{-1}) - 1.1978 (R^2 = 0.9945), revealing that the electrooxidation reaction of glucose at $[VO(acac)_2]$-4-PATP-Au electrode was

followed diffusion controlled electron transfer process. The diffusion coefficient (D) for glucose was 9.5×10^{-6} cm^2/sec and is calculated using the plot (I_{pa} *vs* $\sqrt{\nu}$) and Randles-Sevcik equation $I_p = 2.69 \times 10^5 n^{3/2} A D^{1/2} C \nu^{1/2}$ .....(Eq. 1) [48] where, I_p is the peak current, n is the number of electrons transferred, A is the electrode area, C is the concentration of electroactive species, and ν is the scan rate, considering a temperature of 298 K. The electron transfer coefficient for the totally irreversible oxidation of glucose at $[VO(acaca)_2]$-4-PATP-Au can be determined from equation $E_p - E_{p/2} = 1.857RT/\alpha F = 47.7/\alpha$ mV .....(Eq.2) [48] where E_p and $E_{p/2}$ represent the peak potential and the half-height peak potential, respectively in cyclic voltammetry experiment where R, T and F have their usual meaning. For glucose oxidation, $E_p - E_{p/2}$ = 38 mV, hence electron transfer coefficient (α) is calculated to be 0.63.

The standard heterogeneous rate constant (k_s) for the irreversible oxidation of glucose at $[VO(acac)_2]$-4-PATP-Au electrode was calculated by using the Velasco equation [49] $k_s = 1.11 D^{1/2}(E_p - E_{p/2})^{-1/2}\nu^{1/2}$ ……(Eq.3). The estimated k_s values for totally irreversible oxidation of glucose at $[VO(acac)_2]$ modified electrodes was found to be 5.5×10^{-3} cm/s. The observed higher k_s value for glucose at the modified electrode indicates that the oxidation of glucose was faster at the $[VO(acac)_2]$-4-PATP modified gold electrode. The kinetic parameters for the reduction of H_2O_2 were also calculated (as described for glucose): n = 2, α = 0.69, D = 10.6×10^{-6} cm^2/s and k = 3.3×10^{-3} cm/s.

4.3.5. Effect of accumulation potential and time

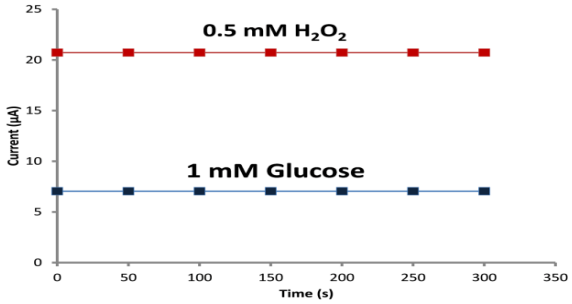

Fig. 4.16. Plot of accumulation time *versus* oxidation peak current of glucose and reduction peak current of H_2O_2 in 0.1 M PBS at pH 7 at $[VO(acac)_2]$-4-PATP-Au electrode.

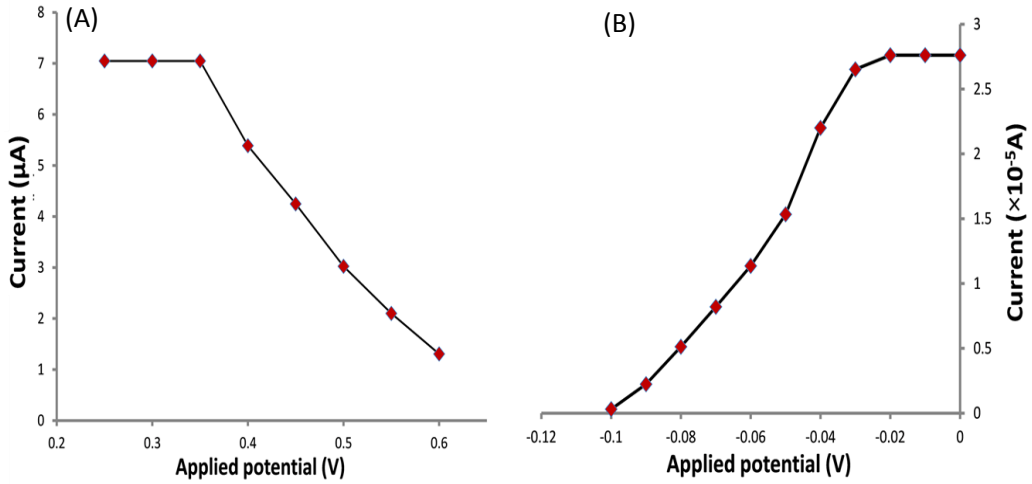

Fig. 4.17. (A) Plot of applied potential *versus* oxidation peak current of 0.1 mM glucose in 0.1 M PBS (pH 7) at $VO(acac)_2$-4-PATP-Au electrode. (B) Plot of applied potential *versus* reduction peak current of 0.5 mM H_2O_2 in 0.1 M PBS (pH 7) at $VO(acac)_2$-4-PATP-Au electrode.

The effect of accumulation time and potential on the oxidation behaviour of glucose and reduction of H_2O_2 at $[VO(acac)_2]$-4-PATP-Au electrode was investigated. Fig. 4.16 shows that the oxidation peak current of glucose and H_2O_2 which were remaining constant with increasing accumulation time from 0-300 sec. Therefore the accumulation time of 60 sec was chosen as the optimum time for further study in both cases. In addition, the influence of accumulation potential on the peak current was examined (Fig. 4.17A and 4.17B) over the potential range 0.0 to 6.0 V for glucose and 0.0 to - 0.5 V for H_2O_2. The peak current for glucose was decreased by changing accumulation potential to more positive value and is due to the oxidation of glucose during the accumulation step at potential higher than that 0.35 V (Fig. 4.17A) where as in case of H_2O_2, by changing accumulation potential to more negative value and is due to the reduction of H_2O_2 during the accumulation step at potential lower than that - 0.02 V (Fig. 4.17B). In fact, the maximum observed current were equal to those observed for open circuit accumulation.

4.3.6. Effect of pH

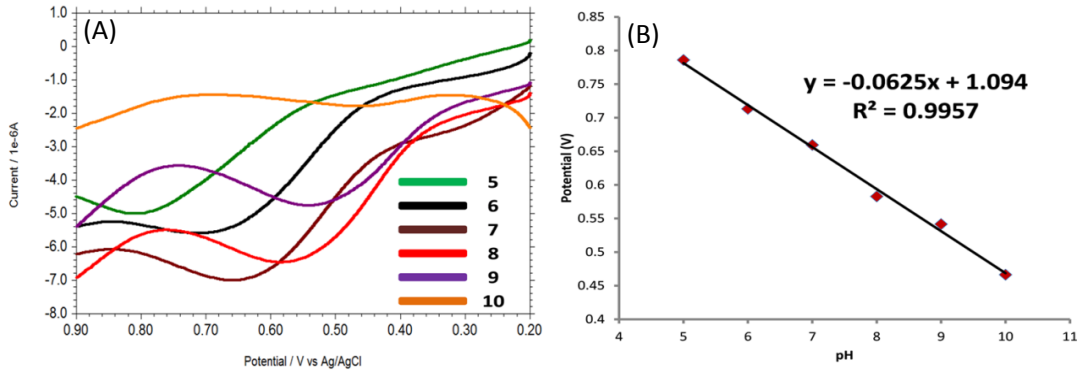

Fig. 4.18. (A) Overlaid DPV of 0.1 mM glucose at different pH using $[VO(acac)_2]$-PATP-Au electrode (B) Plot of oxidation peak potential of 0.1 mM glucose *versus* pH.

The effect of pH on the electrooxdation of glucose and H_2O_2 ware also investigated in the range of pH 5.0 -10.0. As shown in Fig. 4.18A the oxidation peak potential of glucose were pH dependent and was shifted towards more negative potential with increments in

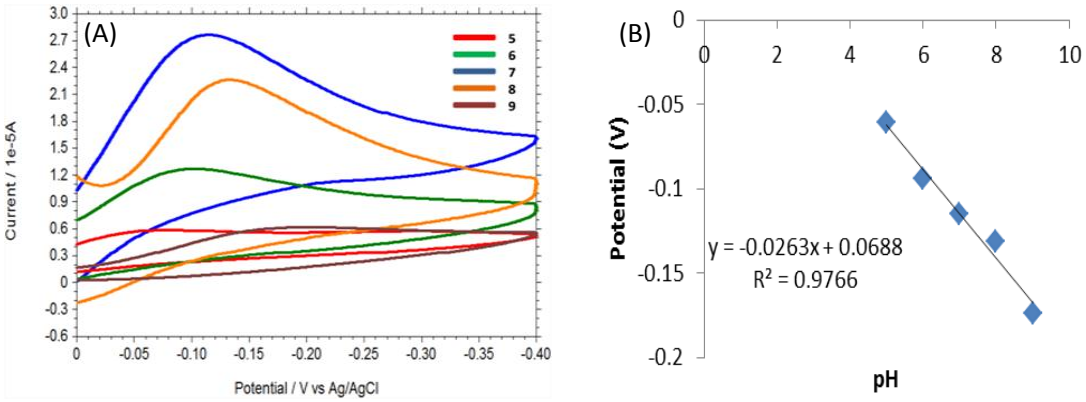

Fig. 4.19. (A) Overlaid CV of 0.5 mM H_2O_2 at different pH obtained with $[VO(acac)_2]$-4-PATP-Au electrode in 0.1 M PBS. (B) Plot of reduction peak current of 0.5 mM H_2O_2 *versus* pH.

solution pH following the linear regression equation of E_{pa} (V) = - 0.0625 pH + 1.094 (R^2 = 0.9957). The slope of 62.5 mV/pH indicated that equal numbers of protons and electrons were involved in the electrode reaction process.[50] Similarly, in Fig. 4.19 the reduction peak potential of H_2O_2 were also pH dependent and that they shifted toward

more positive potential with increments in solution pH following the linear regression equation of E_{pa} (V) = - 0.026 pH + 0.068 (R^2 = 0.976). Investigation of the influence of

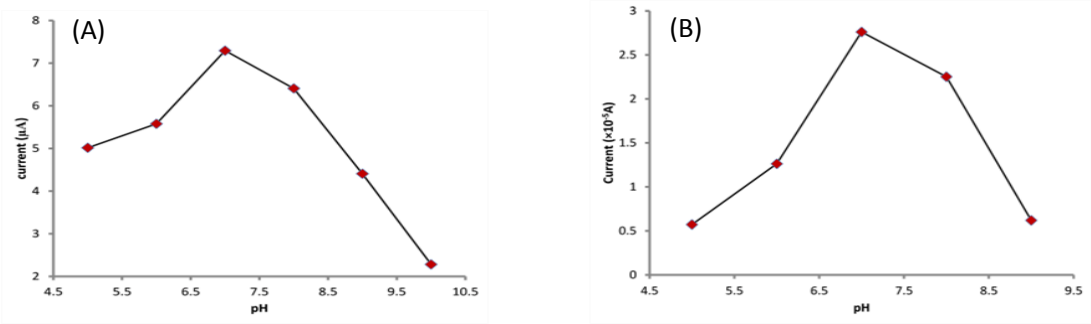

Fig. 4.20. (A) Plot of oxidation peak current of 0.1 mM glucose *versus* pH at $[VO(acac)_2]$-4-PATP-Au electrode in 0.1 M PBS. (B) Plot of reduction peak potential of 0.5 mM H_2O_2 *versus* pH at $[VO(acac)_2]$-4-PATP-Au electrode in 0.1 M PBS.

pH on the peak current of glucose and H_2O_2 at the modified electrode revealed that peak current of glucose and hydrogen peroxide reached a maximum at pH 7.0 and then decreased by increasing pH of the solution (Fig. 4.20 A, B).

4.3.7. Reproducibility, sensitivity and stability

A reproducible and long-term stable electrochemical sensor is highly desirable for the practical application and commercialization. The reproducibility of the $[VO(acac)_2]$-4-PATP-Au electrode was examined by 10 repetitive measurements for glucose and H_2O_2 in 0.1 M PBS solution. The results showed that the anodic peak current for glucose and cathodic peak current for hydrogen peroxide remains same with a relative standard deviation (RSD) of 0.2 and 0.3 %, respectively, indicating that the modified electrode has a good reproducibility. The modified electrode was highly sensitive towards glucose and H_2O_2 and the sensitivity was 120.24 μA cm^{-2} mM^{-1} and 326.66 μA cm^{-2} mM^{-1} for glucose and hydrogen peroxide, respectively.

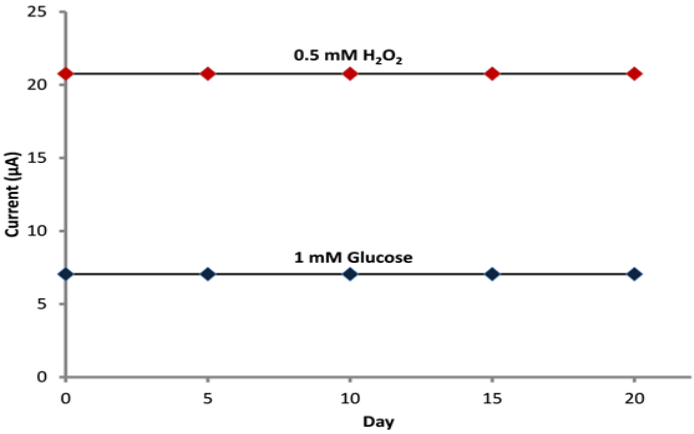

Fig. 4.21. Plot of electrocatalytic current obtained for glucose and hydrogen peroxide with time using $[VO(acac)_2]$-4-PATP-Au electrode.

To further explore the long-term stability, measurements were made with five days intervals (when not in use, the sensor was stored at room temperature using a rubber cap). The sensor retained 100 % of its original current response after 20 days both for glucose (1.0 mM) and H_2O_2 (0.5 mM) in 0.1 M PBS at $[VO(acac)_2]$-4-PATP-Au (Fig. 4.21).

4.3.8. Interference study

In the electrochemical detection of glucose and H_2O_2, the elimination of interferences is a real challenge. Ascorbic acid, uric acid, citric acid, levodopa, cysteine, and different common ions are the major potential interfering agents in the physiological system. In the present study 0.1 mM glucose in presence of 10 fold excess interferents were used at + 0.65 V. The resulting amperograms are shown in Fig. 4.22. There is no obvious current response observed with the addition of these interfering substances, however, an obvious current response with the addition of glucose was appeared (Fig. 4.22A). In addition, the influence of those co-existing electroactive species in the amperometric determination of H_2O_2 was also studied. The working potential was held at – 0.11 V. The amperogram (Fig. 4.22B) shows that all the potential interferents mentioned did not affect the sensor selectivity for H_2O_2. These results suggest that the interfering effect caused by these electroactive species is quite negligible, indicating the highly selective detection of glucose and H_2O_2 at the oxovanadium complex modified electrode.

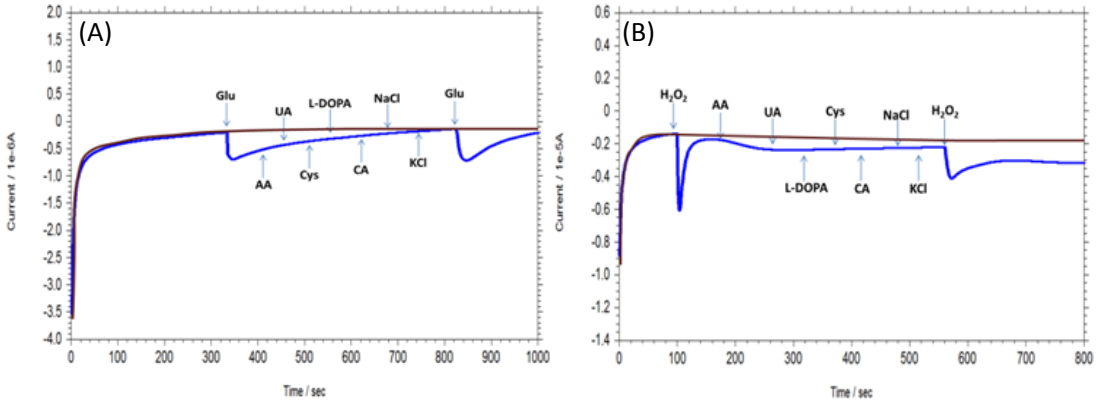

Fig. 4.22. Amperometric response of 0.1 mM glucose at an applied potential of + 0.65 V (A) and 0.1 mM H_2O_2 at an applied potential of - 0.11 V (B) at $[VO(acac)_2]$-4-PATP-Au electrode on subsequent addition, 1.0 mM AA, 1.0 mM UA, 1.0 mM Cys, 1.0 mM l-Dopa, 1.0 mM CA, 1.0 mM NaCl, 1.0 mM KCl, 0.1 mM glucose under stirring condition. (Supporting electrolyte: 0.1 M PBS (pH 7.0), Brown curve shows background current)

4.3.9 Real sample analysis

To testify the feasibility of $[VO(acac)_2]$-4-PATP-Au in real sample analysis, human blood sample (after fasting) was taken for glucose determination whereas processed milk was chosen for the determination of H_2O_2. Before testing, the blood and milk samples were half diluted by 0.1 M phosphate buffer solution.

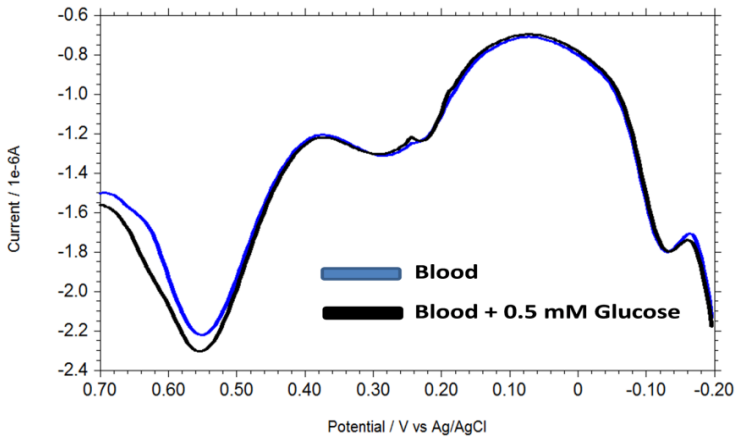

Fig. 4.23. Overlaid DPVs of human blood sample solution and after addition of standard glucose solution in blood sample solution.

Fig. 4.23 shows the overlaid DPV of blood sample solution in PBS (pH 7.6) and after addition of standard glucose solution in blood sample solution. The DPV of blood sample clearly shows the oxidation of glucose at + 0.56 V. The content of glucose in blood sample (5.01 mM = 90.258 mg/dL) was calculated using the standard addition method and the direct interpolation of the linear regression (RSD = 2.24%). A normal fasting (no food for eight hours) blood sugar level is between 70 - 99 mg/dL and by comparing our result was in the similar range. The accuracy of the method was also verified by recovery studied adding standard glucose solution to the real sample and 100.2 % recoveries were obtained. The H_2O_2 concentration in the milk sample was determined as 0.91 μM (= 0.003 mg/dL), using a standard addition method (RSD = 2.16 %), with the recovery of 101.0 %. The results are summarized in Table 4.2. The results indicate that the modified electrode can effectively detect glucose in human blood and hydrogen peroxide in processed milk.

Table 4.2. Determination of glucose in blood sample and H_2O_2 in processed milk with $[VO(acac)_2]$-4-PATP modified gold electrode.

Analyte	**Sample**	**Detected**	**Spiked**	**Found**	**RSD[a] (%)**	**Recovery (%)**
Glucose	Blood	5.01 mM	0.5 mM	0.51 mM	2.24	100.2
H_2O_2	Milk	0.91 μM	1 μM	1.01 μM	2.16	101.0

[a] Five times measurement were taken.

4.4. Conclusions

A unique non-enzymatic electrochemical sensor $[VO(acac)_2]$-4-PATP-Au was developed and used for the detection of glucose and hydrogen peroxide in pure, presence of interferents and real sample. The modified electrode was characterized by microscopic

and electrochemical techniques. Cyclic voltammetry, differential pulse voltammetry, electrochemical impedance spectroscopy, amperometry, chronoamperomery was used for sensing, quantification and determination of kinetic parameters. Till date very limited number of transition metal complex modified electrode has been used for non-enzymatic sensing of glucose and hydrogen peroxide. The novelty of our work is that the same oxovanadium complex modified electrode can detect both glucose as well as hydrogen peroxide. Only few nanoparticles modified electrode has been reported those are able to detect both glucose and hydrogen peroxide. But their preparation process, stability, detection limit, cost are not so impressive. The advantage of our system are easy to prepare, have good selectivity, sensitivity, stability, reproducibility, low detection limit and most importantly cheap than the earlier reported systems. The sensor was efficiently detected glucose in blood sample and hydrogen peroxide in processed milk with good recovery. The new non-enzymatic sensor can be useful for clinical diagnosis and food industry in near future.

4.5. References

1. T. Audesirk, G. Audesirk, *Biology, Life on Earth*, 5th Edition, Prentice-Hall, 1999.
2. J. Webster (Ed.) *Medical Instrumentation Application and Design*, 4th Edition. Wiley Hoboken, NJ, 2009.
3. B. J. Privett, J. H. Shin and M. H. Schoenfisch, *Anal. Chem.*, 2008, ***80***, 4499.
4. M. Zhou, Y. Zhai and S. Dong, *Anal. Chem*., 2009, **81**, 5603.
5. M. Giorgio, M. Trinei, E. Migliaccio and P.G. Pelicci, *Nat. Rev. Mol. Cell Biol*., 2007, **8**, 722.
6. C. Laloi, K. Apel and A. Danon, *Curr. Opin. Plant Biol.*, 2004, **7**, 323.
7. N. V. Klassen, D. Marchington and H. C. E. McGowan, *Anal. Chem.*, 1994, **66**, 2921.
8. Z. H. Li, D. H. Li, K. Oshita and S. Motomizu, *Talanta*, 2010, **82**, 1225.
9. T. Jiao, B. D. Leca-Bouvier, P. Boullanger, L. J. Blum and A. P. Girard-Egrot, *Colloids Surf. A*, 2008, **321**, 143.
10. B. Haghighi and S. Bozorgzadeh, *Microchem. J*, 2010, **95**, 192.
11. Y. Shen, M. Trauble and G. Wittstock, *Anal. Chem*., 2008, **80**, 750.
12. S. H. Lim, J. Wei, J. Lin, Q. Li, and J. KuaYou, *Biosens. Bioelectron.*, 2005, **20**, 2341.
13. M.-Y. Hua, Y.-C. Lin, R.-Y. Tsai, H.-C. Chen and Y.-C. A. Liu, *Microchim. Acta*, 2011, **56**, 9488.
14. A. A. Ensafi, M. Jafari-Asl, N. Dorostkar, M. Ghiaci, M. Victoria Mart´ınez-Huerta and J. L. G. Fierro, *J. Mater. Chem. B*, 2014, **2**, 706.
15. Y. Li, Y. Zhong, Y. Zhang, W. Weng and S. Li, *Sens. Actuators B*, 2015, **206**, 735.
16. Y. Wang and F. Caruso, *Chem. Commun*., 2004, 1528.
17. K. E. Toghill and R. G. Compton, *Int. J. Electrochem. Sci*., 2010, **5**, 1246.
18. S. Park, H. Boo, and T.D. Chung, *Anal. Chim. Acta*, 2006, **556**, 46.
19. P. Yang, X.Tong, G. Wang, Z. Gao, X. Guoand and Y. Qin, *ACS Appl. Mater. Interfaces*, 2015, **7**, 4772.
20. P. Si, X. C. Dong, P. Chen and D. H. Kim, *J. Mater. Chem. B*, 2013, **1**, 110.

21. Y. Li, Y. Zhonga, Y. Zhanga, W. Wenga, S. Li, *Sens. Actuators B,* 2015, **206**, 735.
22. K. K. Lee, P.Y. Loh, C. H. Sow and W. S. Chin, *Biosens. Bioelectron.,* 2013, **39**, 255.
23. L. Ozcan, Y. Sahin and H. Turk, *Biosens. Bioelectron.,* 2008, **24**, 512 -17.
24. M. Y. Elahi, H. Heli, S. Z. Bathaie and M.F. Mousavi, *J. Solid State Electrochem.,* 2007, **11**, 273.
25. M. d. S. M. Quintino, H. Winnischofer, M. Nakamura, K. Araki, H. E. Toma and L. Angnes, *Anal. Chim. Acta,* 2005, **539**, 215.
26. G. Sivasankari, C. Priya and S.S. Narayanan, *Int. J. Pharm. Bio. Sci.*, 2012, **2**, 188.
27. C. S. Shen, Y. Z. Wen, Z.L. Shen, J. Wu and W. P. Liu, *J. Hazard Mater.*, 2011, **193**, 209.
28. M. d. S. M.Quintino, H. Winnischofer, K. Araki, H.E. Toma, L. Angnes, *Analyst*, 2005, **130**, 221.
29. X. Zeng, X. Liu, B. Kong, Y. Wang and W. Wei, *Sens. Actuators B,* 2008, **133**, 381.
30. D. C. Crans, J. J. Smee and E. Gaidamauskas, L. Yang, *Chem. Rev*., 2004, **104**, 849.
31. C.C. Lee, y. L. Hu and M. W. Ribbe, *Proc. Natl. Acad. Sci.* U.S.A., 2009, **106**, 9209; R. Wever and M. A. Van der Horst, *Dalton Trans*., 2013, **42**, 11778.
32. A. Bulter, *Coord. Chem. Rev*., 1999, **187**, 17.
33. G. J. Ligtenbarg, R. Hage and B. L. Feringa, *Coord. Chem. Rev.*, 2003, **237**, 89.
34. D. Talukdar, K. Sharma, S.K. Bharadwaj and A. Thakur, J. *Synlett.,* 2013, **24**, 963.
35. L. Rout, T. Punniyamurthy, *Adv. Synth. Catal*., 2005, **347**, 1958.
36. S. Raghavan, A. Rajender, S.C. Joseph and M.A. Rasheed, *Synth. Commun*., 2001, **31**, 1477.
37. M. Aschi, M. Crucianelli, A. D. Giuseppe, C. D. Nicola and F. Marchetti, *Catl. Today,* 2012, **192**, 56.

38. T. Itoh, K. Jitsukawa, K. Kaneda and S. Teranishi, *J. Am. Chem. Soc*., 1979, **101**, 159.
39. C-Y. Chu, D-R. Hwang, S-K. Wang and B-J. Uang, *Tamkang J. Sci. Eng*., 2003, **6**, 65.
40. K. H. Thomson, J. Lichter, C. LeBel, M. C. Scaife, J. H. McNeill and C. Orvig, *J. Inorg. Bioch*., 2009, **103**, 554.
41. M. W. Makinen and M. Salehitazangi, *Coord. Chem. Rev.,* 2014, **279**, 1.
42. S. Kadota, I. G. Fantus, G. Deragon, H. J. Guyda and B. I. Posner, *J. Biol. Chem.*, 1987, **262**, 8252.
43. M. W. Makinen and M. J. Brady, *J. Biol. Chem*., 2002, **277**, 12215.
44. J. F. Smalley, K. Chalfant, S. W. Feldberg, T. M. Nahir and E. F. Bowden, *J. Phys. Chem. B*, 1999, **103**, 1676.
45. H. O. Finklea, S. Avery, M. Lynch and J. Furtsch, *Langmuir*, 1987, **3**, 409.
46. K. Barman and Sk. Jasimuddin, *Catal. Sci. Technol*., 2015, **5**, 5100.
47. L. Zhang and S. Dong, *J. Electroanal. Chem*., 2004, **568,** 189.
48. A.J. Bard and L. R. Faulkner, *Electrochemical Methods: Fundamental and Applications*, John Wiley & Sons Inc., New York, 2001.
49. J. G. Velasco, *Electroanalysis*, 1997, **9**, 880.
50. E. Laviron, *J. Electroanal. Chem.*, 1974, **52**, 355.